CHEMISTRY OF MATERIALS

Communication

pubs.acs.org/cm

Identifying the Discharge Product and Reaction Pathway for a Secondary Mg/O_2 Battery

Gulin Vardar,[†] Emily G. Nelson,[‡] Jeffrey G. Smith,[§] Junichi Naruse,[∥] Hidehiko Hiramatsu,[⊥] Bart M. Bartlett,[‡] Alice E. S. Sleightholme,[#] Donald J. Siegel,*[,†,§,▽] and Charles W. Monroe*[,#,⊗]

[†]Materials Science and Engineering Department, [‡]Chemistry Department, [§]Mechanical Engineering Department, and [#]Chemical Engineering Department, University of Michigan, Ann Arbor, Michigan 48109, United States

[∥]North America Research & Development, DENSO International America, Inc., 24777 Denso Drive, Southfield, Michigan 48086, United States

[⊥]Research Laboratories, DENSO CORPORATION, 500-1, Minamiyama, Komenoki-cho, Nisshin 470-0111, Japan

[▽]Department of Energy Conversion and Storage, Technical University of Denmark, Fysikvej, Building 309, 2800 Kgs Lyngby, Denmark

[⊗]Department of Engineering Science, University of Oxford, Parks Road, Oxford OX1 3PJ, United Kingdom

Supporting Information

Nonaqueous metal/oxygen batteries exhibit high theoretical specific energy densities.[1] Chemistries based on alkali metals, such as Li/O_2, Na/O_2, and K/O_2, have become popular research topics because they also hold promise for rechargeability.[2−6] Multivalent battery systems involving alkaline earth metals, such as the Mg/O_2 chemistry, can achieve higher theoretical energy densities than some of their alkali-metal analogues but have received little research emphasis.[7,8] Although aqueous primary Mg/O_2 batteries have been demonstrated, their cell potentials are limited by the presence of water; moreover, corrosion of the Mg electrode likely precludes rechargeability.[9−12] Nonaqueous electrolytes could enable a reversible Mg/O_2 cell, however.

The secondary Mg/O_2 battery is particularly attractive among multivalent options. In a Mg/O_2 cell, the half-reactions

$$Mg^{2+} + O_2 + 2e^- \rightleftharpoons MgO_2 \ (2.91\ \text{V vs}\ Mg^{2+/0}) \quad (1)$$

$$2Mg^{2+} + O_2 + 4e^- \rightleftharpoons 2MgO \ (2.95\ \text{V vs}\ Mg^{2+/0}) \quad (2)$$

might be anticipated at the gas electrode. Both involve Mg^{2+} ions and dissolved O_2 from the liquid electrolyte, and both promise moderately high cell potentials of ∼2.9 V. A Mg/O_2 cell with a MgO discharge product formed by half-reaction 2 would exhibit theoretical maximum volumetric and gravimetric energy densities of approximately 14 kWh L^{-1} and 3.9 kWh kg^{-1}, respectively, surpassing Li/O_2 cells that discharge to Li_2O_2 (8.0 kWh L^{-1} and 3.4 kWh kg^{-1}).[1]

Despite the possible benefits relative to alkali-metal chemistries, many details critical to Mg/O_2 cell performance remain poorly understood, including the composition of the discharge product and the factors that facilitate recharge.[7,8,13] In any metal/O_2 system, the properties of the discharge product (typically a metal oxide, peroxide, or superoxide) can strongly influence cell performance. The discharge phase's composition and structure impact overall energy density, whereas its transport properties[14−18] and chemistry with the electrolyte[19] may also control effective capacity and cycle life.[20,21] The Na/O_2 system provides a stark example of how product stoichiometry can impact energy efficiency: Na/O_2 cells that discharge to Na_2O_2 exhibit high overpotentials during charging; those that discharge to NaO_2 do not.[3,22−24]

Shiga et al. reported a nonaqueous Mg/O_2 cell involving an iodine−dimethyl sulfoxide (I_2-DMSO) redox shuttle that operates at elevated temperature (60 °C).[7] The shuttle facilitated recharging, and operation at elevated temperatures enabled reversible plating and stripping of metallic Mg. The discharge product was assumed to be MgO because charging capacity increased for a positive electrode preloaded with MgO. A discharge voltage of ∼1.25 V was observed (at 0.78 mA cm^{-2} superficial).

For the present report, Mg/O_2 cycling experiments were performed using cells specifically designed for metal/O_2 testing, depicted in the Supporting Information (SI) Figure S1. Cell fabrication and disassembly, as well as transfer procedures for characterization, closely followed the procedures described earlier by Griffith et al.[25] Mg/O_2 cells (EL-CELL Gmbh, Germany) were constructed by sandwiching a glass-fiber separator (0.5 mm thick, EL-CELL Gmbh, Germany) between a planar metallic-Mg negative electrode (99.9%, Goodfellow, USA) and a porous-carbon positive electrode (SIGRACET GDL 24 BC, Ion Power, Inc., USA). A stainless-steel plate with 1.5 mm diameter perforations (EL-CELL Gmbh, Germany) acted as a positive current collector, and was coated with evaporatively deposited Pt to prevent corrosion during cell testing. The perforations in the plate allowed contact between the carbon and stagnant O_2 (99.993%, Cryogenic Gases, USA; 2 bar absolute). The separator and carbon were saturated with an electrolyte comprising a 4:1 mol ratio of phenylmagnesium chloride:aluminum phenoxide in tetrahydrofuran (THF), which was produced using the precursor materials and following the synthesis procedure described by Nelson et al.[26] The $(PhMgCl)_4$−$Al(OPh)_3$/THF electrolyte allows Mg plating and stripping at room temperature with high Coulombic efficiency, and its apparent oxidative stability is higher than 4 V vs $Mg^{2+/0}$ against

Received: September 14, 2015
Revised: November 6, 2015
Published: November 6, 2015

DOI: 10.1021/acs.chemmater.5b03608
Chem. Mater. 2015, 27, 7564−7568

both Pt and C (SI, Figures S2 and S3).[26] Charge/discharge experiments were performed at room temperature using a series 4000 battery tester (Maccor, USA). Additional experimental details are provided in the SI.

Each Mg/O_2 cell was held at open circuit under O_2 until the measured voltage equilibrated, typically yielding an open-circuit potential (OCP) of 2.0 ± 0.1 V (see SI, Figure S4). This OCP is low compared to the theoretical potentials expected from half-reactions 1 or 2.

Figure 1 compares the half-reaction potentials for the Mg/O_2 system with the accepted half-reaction potentials of various

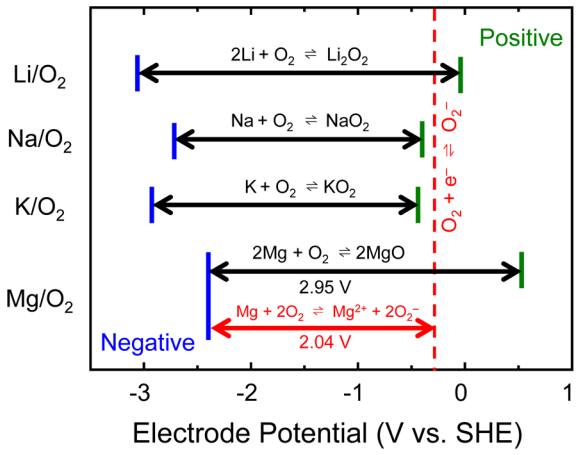

Figure 1. Cell potentials and half-reaction potentials for several metal/O_2 battery chemistries. The dashed red line corresponds to the potential at which O_2 reduces to superoxide.

alkali-metal/O_2 chemistries. In all cases, cells based on alkali metals exhibit OCPs close to the theoretical potentials expected for positive-electrode half-reactions involving the direct electrochemical formation of M_xO_y compounds from metal cations and O_2.[3,4,27] As Figure 1 shows, however, the potential associated with superoxide formation ($O_2 + e^- \rightleftharpoons O_2^-$, −0.33 V vs SHE) in the alkali chemistries also closely matches the potentials for direct electrochemical M_xO_y formation from Li, Na, and K, making identification of the reaction pathway more challenging. In contrast, for Mg/O_2, superoxide forms from O_2 far (~0.9 V) below the potential for direct electrochemical MgO or MgO_2 formation.

In light of the thermodynamic data summarized in Figure 1, the OCP in the Mg/O_2 system suggests a reaction pathway where oxygen reduction (i.e., O_2^- formation) occurs as an initial electrochemical step: superoxide formation precedes a chemical reaction with Mg^{2+} that forms MgO_2 and liberates molecular O_2, after which MgO_2 disproportionation occurs:

$$O_2 + e^- \rightleftharpoons O_2^- \ (2.04\ \text{V vs } Mg^{2+/0}) \quad (3a)$$

$$2O_2^- + Mg^{2+} \rightleftharpoons MgO_2 + O_2 \quad (3b)$$

$$2MgO_2 \rightleftharpoons 2MgO + O_2 \quad (3c)$$

This hypothesized pathway is an ECC ("electrochemical-chemical-chemical") mechanism similar to those proposed for Li/O_2 and other alkali-metal-based systems.[28−31] Below, the results of several characterization techniques confirm that the discharge-product composition is also consistent with this ECC mechanism.

Unlike alkali-metal/O_2 systems, superoxide formation in Mg/O_2 cells occurs at a low enough potential to distinguish step 3a from direct electrochemical formation of MgO_x (reactions 1 and 2). The subsequent chemical steps that form MgO_2 and MgO do not contribute to the electrical work delivered by the cell. Materials that select against the superoxide pathway and support direct electrochemical formation of MgO_x will be needed to realize the promise that the Mg/O_2 chemistry holds for higher energy density.

Figure 2 shows discharge/recharge cycles for a typical Mg/O_2 cell. During discharge, the voltage decreases monotonically until

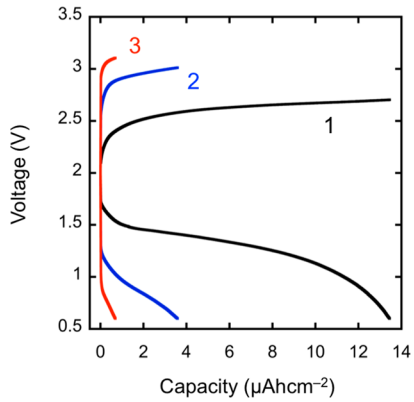

Figure 2. Discharge/recharge cycles for a room-temperature Mg/O_2 cell at 5 μA cm^{-2} (superficial). Curves are labeled with the corresponding cycle numbers.

reaching the 0.6 V cutoff. At the end of discharge the cell is allowed to equilibrate for 30 min before recharging. Once a charging current is applied, the voltage quickly jumps to 2.5 V, and then rises monotonically until the discharge capacity is recovered. The energy efficiency for the first cycle is 42%—low compared to the energy efficiencies reported for nonaqueous Li/O_2, K/O_2 and Na/O_2 chemistries, but comparable to those for elevated-temperature Mg/O_2 cells.[3,4,7,32] Still, the average overpotentials during the discharge and recharge processes are similar, suggesting that the electrochemical steps involved in the forward and reverse cell reactions have similar activation energies. Upon cycling, the capacity fade compares with other reported nonaqueous Mg/O_2 systems.[7,8] The cell capacity is low, probably owing to the low solubility and diffusivity of O_2 in the electrolyte.[33] The solubility of O_2 in THF is about 5 times lower than in dimethoxyethane, a common metal/O_2 battery solvent.[34,35] The measured conductivity of the present electrolyte was reported by Nelson et al. to be 1.24 mS cm^{-1},[26] which is comparable to other Mg electrolytes[36−39] but almost 1 order of magnitude smaller than typical lithium-battery electrolytes.[40,41] Development of an electrolyte with higher O_2 solubility and ionic conductivity could facilitate improvements in both the capacity and rate capability of the Mg/O_2 chemistry.

The total discharge-product volume can be estimated by extrapolating the particle coverage in Figure S7 across the whole electrode. This volume of MgO corresponds to a charge capacity of the same order as the measured capacity. Of course, a capacity estimate based on discharge-product dimensions is at best qualitative; such an estimate is presented only to demonstrate consistency with the more accurate capacities determined by discharge experiments.

To probe possible side reactions, discharge was attempted in an Ar atmosphere (i.e., in a cell containing no O_2). In this case,

DOI: 10.1021/acs.chemmater.5b03608
Chem. Mater. 2015, 27, 7564−7568

the measured OCP was roughly half that of the O_2-containing cell, 1.0 ± 0.1 V (Figure S4). Upon discharge, the voltage monotonically decreased (Figure S5), suggesting that there is a side-reaction below 1 V that may arise from solvent degradation. Side reactions at low voltages are also observed in the Li/O_2 system.[42]

In preparation for imaging by scanning electron microscopy (SEM), the positive electrodes were rinsed with THF in an Ar-atmosphere glovebox to remove residual electrolyte and placed in the airtight sample holder described by Griffith et al.[25] Figure 3a,b shows SEM images of the oxygen-electrode surface after discharge. Discharge product is concentrated within areas of the electrode that were in direct contact with O_2 through the perforations in the current collector. The product comprises large, faceted, transparent particles, which have characteristic dimensions of 100−200 μm. These particles were only observed on the side of the positive electrode exposed to O_2. Absence of the discharge product in areas further from the O_2 supply indicates that O_2 permeation through the liquid electrolyte limits capacity. A control image [Figure 3b inset] was generated by holding a similar cell at open circuit under O_2 for the same duration as the discharge experiment (a larger area is shown in Figure S8). No particles were observed on the control electrode. Figure 3c,d shows that a majority of the particles have decomposed at the end of first recharge. The incomplete disappearance of the discharge product suggests the presence of side reactions, which may rationalize both the low energy efficiency and the capacity fade upon cycling.

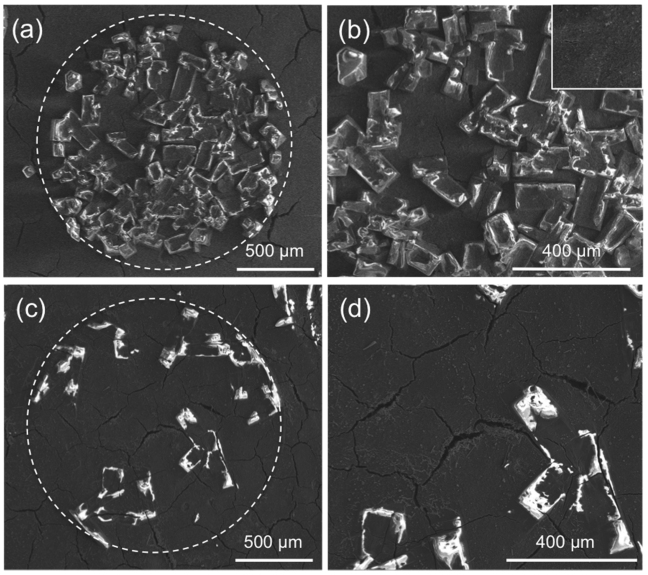

Figure 3. SEM images of the positive-electrode surface on the side closest to the O_2 gas inlet. The dashed circles represent boundaries of the regions that were directly exposed to O_2 through perforations in the Pt-coated current collector. (a) An electrode after first discharge. (b) Higher magnification of the first-discharge product, with an inset image of a control electrode exposed to O_2 in a cell held at open circuit. (c) An electrode at the end of first recharge. (d) Higher magnification of the residual product after first recharge.

In addition to SEM, the composition of the discharge product was characterized using energy dispersive X-ray spectroscopy (EDS), Auger electron spectroscopy (AES), X-ray diffractometry (XRD), and Raman spectroscopy (RS). Results of AES, XRD, and RS are shown in Figure 4; EDS data is presented in the SI, Figure S10.

EDS suggested the presence of Mg, O, and Cl in the discharge product. In agreement with the EDS results, AES also showed signals for only Mg, O, and Cl (Figure S12). The Mg peak is located at 1181.5 eV, in agreement with the Mg $KL_{2,3}L_{3,3}$ Auger energy of Mg in MgO.[43] In contrast to the EDS measurement, samples analyzed by AES were briefly exposed to air during sample transfer. Therefore, AES was performed in conjunction with Ar sputtering to remove the exterior surface of the discharge product. Figure 4a shows the atomic-composition percentages with respect to the distance from the surface yielded by an AES depth profile. The results suggest a MgO_x stoichiometry with $x > 1$. Furthermore, AES reveals that the quantity of Cl in the discharge product is small (average ~3.1 at. %); this trace Cl presumably owes to a reaction with the electrolyte. It is noteworthy that the proportions of Mg, O, and Cl remain relatively constant with respect to depth. The excess of O can be explained by the presence of domains of MgO_2 within the predominantly MgO material. The Mg−O phase diagram indicates that MgO is a line compound, and is the only stable Mg−O compound at ambient conditions.[44] On the basis of the theoretical potentials from eqs 1 and 2, MgO_2 has a less exergonic formation energy than MgO (by ~0.08 eV/formula unit); it is therefore weakly metastable and does not appear in the equilibrium phase diagram. Thus, the presence of MgO_2 in the discharge product likely owes to a kinetic effect. If the discharge

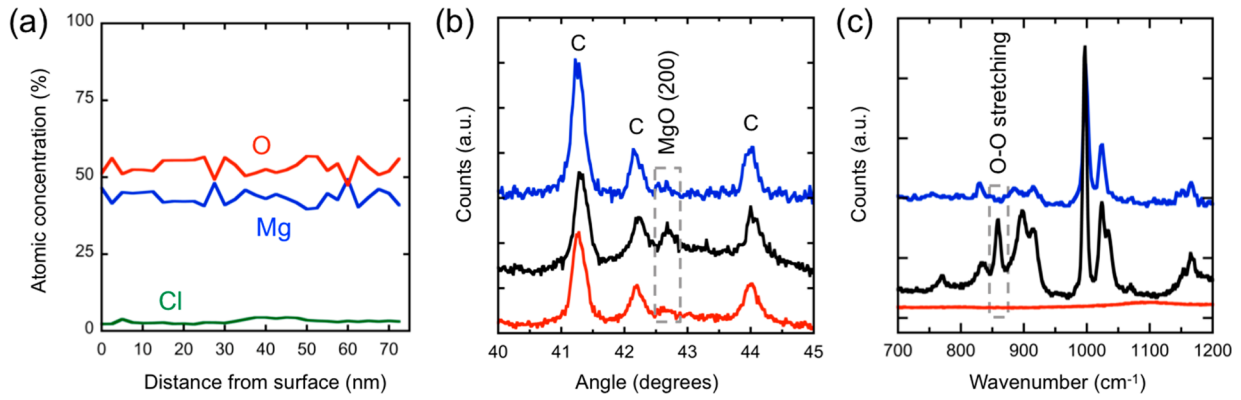

Figure 4. (a) AES depth profile of the discharge product; Mg (Blue), O (red) and Cl (green) atomic concentrations are plotted as functions of sputtering depth. (b) XRD pattern of control (red), discharged (black) and recharged (blue) carbon electrodes. (c) Raman spectra collected from control (red), discharged (black), and recharged (blue) carbon electrodes.

DOI: 10.1021/acs.chemmater.5b03608
Chem. Mater. 2015, 27, 7564−7568

product is assumed to be a physical mixture of MgO and MgO_2, the AES data indicates that ~30% of the product by volume is MgO_2 (SI, Section 6). In contrast to the oxygen-rich composition of the discharge product, particles remaining on the positive electrode after recharge exhibit a 1:1 Mg:O ratio in AES (Figure S12). This suggests that MgO_2 decomposes preferentially during charging. Note that some MgO also must be consumed during the recharge process, because Figure 3c shows that significantly more than 30% of the discharge-product volume is consumed.

Figure 4b shows X-ray diffraction patterns collected from discharged, recharged, and control electrodes. Patterns were collected without exposure to air using an airtight sample holder. The MgO(200) peak appears in the XRD patterns of the discharged and recharged electrodes, but this peak is absent from the control-electrode XRD pattern, confirming that no discharge product forms when the cell is held at open circuit. In the recharged positive electrode, the peak attributed to crystalline MgO is significantly diminished, suggesting substantial, but not complete, dissolution of MgO during charging. No peaks corresponding to crystalline MgO_2 were observed in any electrode.

Absence from the XRD patterns does not preclude the presence of amorphous MgO_2, however. Figure 4c shows Raman spectra collected from the discharge product, the product remaining after recharge, and the control electrode. The oxygen electrodes were placed in an airtight RS sample holder with quartz windows. Several spectra were collected from reference samples to identify the peaks in the discharge-product spectrum (Figure S13). The sharp peaks between 870 and 1100 cm^{-1} all can be assigned to residual electrolyte with THF solvent.[45] The peak around 200 cm^{-1} can be attributed to Mg−Cl stretching (Figure S13). In particular, the peak near 860 cm^{-1} was confirmed to correspond to O−O stretching in MgO_2 by density-functional-theory calculations (Figure S14), and has been attributed to O−O stretching in other peroxide compounds.[46] (MgO does not yield a first-order Raman signal and therefore cannot not be detected by RS.[47]) The observation of a MgO_2 peak in the Raman spectrum confirms the presence of amorphous MgO_2 in the discharge product and is consistent with the excess oxygen observed by AES. In the recharged positive electrode the peak attributed to O−O stretching is not observed, supporting the notion that MgO_2 decomposes preferentially during recharge, and in agreement with the 1:1 Mg:O stoichiometry measured by AES (Figure S12).

In summary, the present study has probed the reaction pathway and characterized the discharge product in a reversible Mg/O_2 cell. Importantly, several aspects of Mg/O_2 electrochemistry appear to differ fundamentally from alkali-metal/O_2 systems. The cell produces a mixed-phase product that comprises crystalline MgO with domains of amorphous MgO_2; this product forms after electrochemical superoxide formation from O_2, through chemical precipitation and disproportionation steps. A discharge product comprising large, faceted particles was observed, but was seen only in areas of the electrode that were in close proximity to gas, suggesting that O_2 transport limits cell capacity. Several techniques probed the discharge-product composition, revealing that the product comprises roughly 70% MgO and 30% amorphous MgO_2 on a volumetric basis. The recharged positive electrode contained a small amount of residual MgO, suggesting that MgO_2 decomposes first during charging, followed by more limited MgO decomposition.

The combination of a multivalent metal with an air-breathing positive electrode portends a secondary battery system with extremely high energy density. The superoxide-controlled discharge voltage, low capacity, and limited cycle life observed for the Mg/O_2 cell presented here suggest that additional development is needed to realize these advantages. Further electrolyte development could increase both capacity and rate performance. In addition, circumventing the multistep discharge mechanism in favor of direct electrochemical MgO_x formation would lead to cells with far higher energy density.

■ ASSOCIATED CONTENT

Supporting Information

The Supporting Information is available free of charge on the ACS Publications website at DOI: 10.1021/acs.chemmater.5b03608.

Additional experimental information, cyclic voltammograms of electrolyte, zero-current hold data, discharge curve for O_2-free cell, calculated Raman spectra for MgO_2, measured reference Raman spectra, EDS of discharge product, and AES data for discharged and recharged positive electrodes (PDF).

■ AUTHOR INFORMATION

Corresponding Authors

*D.J.S. E-mail: djsiege@umich.edu.

*C.W.M. E-mail: charles.monroe@eng.ox.ac.uk.

Notes

The authors declare no competing financial interest.

■ ACKNOWLEDGMENTS

DENSO International America, Inc. provided financial support for this work. The authors thank Zhongrui Li for technical support with AES. D.J.S. acknowledges the Villum Foundation's Visiting Professor Program and the Nordea Foundation's Residence Program for support during his stay at DTU.

■ REFERENCES

(1) Zu, C.-X.; Li, H. Thermodynamic Analysis on Energy Densities of Batteries. *Energy Environ. Sci.* **2011**, *4*, 2614−2624.

(2) Peng, Z.; Freunberger, S. A.; Chen, Y.; Bruce, P. G. A Reversible and Higher-rate Li-O_2 Battery. *Science* **2012**, *337*, 563−566.

(3) Hartmann, P.; Bender, C. L.; Vračar, M.; Dürr, A. K.; Garsuch, A.; Janek, J.; Adelhelm, P. A Rechargeable Room-temperature Sodium Superoxide (NaO_2) Battery. *Nat. Mater.* **2012**, *12*, 228−232.

(4) Ren, X.; Wu, Y. A Low-overpotential Potassium-oxygen Battery based on Potassium Superoxide. *J. Am. Chem. Soc.* **2013**, *135*, 2923−2926.

(5) Bender, C. L.; Hartmann, P.; Vračar, M.; Adelhelm, P.; Janek, J. On the Thermodynamics, the Role of the Carbon Cathode, and the Cycle Life of the Sodium Superoxide (NaO_2) Battery. *Adv. Energy Mater.* **2014**, *4*, 1301863.

(6) Radin, M. D.; Siegel, D. J. Non-Aqueous Metal-Air Batteries: Past, Present, and Future, Chapter 18. In *Rechargeable Batteries: Materials, Technologies and New Trends*; Zhang, Z., Zhang, S. S., Eds.; Springer: Switzerland, 2015; p 511. DOI: 10.1007/978-3-319-15458-9_18.

(7) Shiga, T.; Hase, Y.; Kato, Y.; Inoue, M.; Takechi, K. A Rechargeable Non-aqueous Mg-O_2 Battery. *Chem. Commun. (Cambridge, U. K.)* **2013**, *49*, 9152−9154.

(8) Shiga, T.; Hase, Y.; Yagi, Y.; Takahashi, N.; Takechi, K. Catalytic Cycle Employing a TEMPO−Anion Complex to Obtain a Secondary Mg−O_2 Battery. *J. Phys. Chem. Lett.* **2014**, *5*, 1648−1652.

(9) Sathyanarayana, S.; Munichandraiah, N. A New Magnesium-air Cell for Long-life Applications. *J. Appl. Electrochem.* **1981**, *11*, 33−39.

(10) Khoo, T.; Howlett, P. C.; Tsagouria, M.; MacFarlane, D. R.; Forsyth, M. The Potential for Ionic Liquid Electrolytes to Stabilise the

DOI: 10.1021/acs.chemmater.5b03608
Chem. Mater. 2015, 27, 7564−7568

Magnesium Interface for Magnesium/air Batteries. *Electrochim. Acta* **2011**, *58*, 583−588.
(11) Ma, Y.; Li, N.; Li, D.; Zhang, M.; Huang, X. Performance of Mg−14Li−1Al−0.1Ce as Anode for Mg-air battery. *J. Power Sources* **2011**, *196*, 2346−2350.
(12) Mayilvel Dinesh, M.; Saminathan, K.; Selvam, M.; Srither, S. R.; Rajendran, V.; Kaler, K. V. I. S. Water Soluble Graphene as Electrolyte Additive in Magnesium-air Battery System. *J. Power Sources* **2015**, *276*, 32−38.
(13) Luder, D.; Ein-Eli, Y. Electrochemical Grignard Reagent Synthesis for Ionic-Liquid-Based Magnesium-Air Batteries. *ChemElectroChem* **2014**, *1*, 1319−1326.
(14) Radin, M. D.; Monroe, C. W.; Siegel, D. J. Impact of Space Charge Layers on Sudden Death in Li/O_2 Batteries. *J. Phys. Chem. Lett.* **2015**, *6*, 3017−3022.
(15) Yang, S.; Siegel, D. J. Intrinsic Conductivity in Sodium-air Battery Discharge Phases: Sodium Superoxide vs. Sodium Peroxide. *Chem. Mater.* **2015**, *27*, 3852−3860.
(16) Radin, M. D.; Monroe, C. W.; Siegel, D. J. How Dopants can Enhance Charge Transport in Li_2O_2. *Chem. Mater.* **2015**, *27*, 839−847.
(17) Tian, F.; Radin, M. D.; Siegel, D. J. Enhanced Charge Transport in Amorphous Li_2O_2. *Chem. Mater.* **2014**, *26*, 2952−2959.
(18) Radin, M. D.; Siegel, D. J. Charge Transport in Lithium Peroxide: Relevance for Rechargeable Metal-Air Batteries. *Energy Environ. Sci.* **2013**, *6*, 2370−2379.
(19) Kumar, N.; Radin, M. D.; Wood, B. C.; Ogitsu, T.; Siegel, D. J. Surface-Mediated Solvent Decomposition in Li-air Batteries: Impact of Peroxide and Superoxide Surface Terminations. *J. Phys. Chem. C* **2015**, *119*, 9050.
(20) Das, S. K.; Lau, S.; Archer, L. A. Sodium−oxygen Batteries: a New Class of Metal−air Batteries. *J. Mater. Chem. A* **2014**, *2*, 12623−12629.
(21) Johnson, L.; Li, C.; Liu, Z.; Chen, Y.; Freunberger, S. A.; Tarascon, J.-M.; Ashok, P. C.; Praveen, B. B.; Dholakia, K.; Bruce, P. G. The Role of LiO_2 Solubility in O_2 Reduction in Aprotic Solvents and its Consequences for Li−O_2 Batteries. *Nat. Chem.* **2014**, *6*, 1091−1099.
(22) Sun, Q.; Yang, Y.; Fu, Z.-W. Electrochemical Properties of Room Temperature Sodium−Air Batteries with Non-aqueous Electrolyte. *Electrochem. Commun.* **2012**, *16*, 22−25.
(23) Liu, W.; Sun, Q.; Yang, Y.; Xie, J. Y.; Fu, Z. W. An Enhanced Electrochemical Performance of a Sodium-air Battery with Graphene Nanosheets as Air Electrode Catalysts. *Chem. Commun. (Cambridge, U. K.)* **2013**, *49*, 1951−1953.
(24) Yadegari, H.; Li, Y.; Banis, M. N.; Li, X.; Wang, B.; Sun, Q.; Li, R.; Sham, T.-K.; Cui, X.; Sun, X. On Rechargeability and Reaction Kinetics of Sodium−air Batteries. *Energy Environ. Sci.* **2014**, *7*, 3747−3757.
(25) Griffith, L. D.; Sleightholme, A. E.; Mansfield, J. F.; Siegel, D. J.; Monroe, C. W. Correlating Li/O_2 Cell Capacity and Product Morphology with Discharge Current. *ACS Appl. Mater. Interfaces* **2015**, *7*, 7670−7678.
(26) Nelson, E. G.; Brody, S. I.; Kampf, J. F.; Bartlett, B. M. A Magnesium Tetraphenylaluminate Battery Electrolyte Exhibits a Wide Electrochemical Potential Window and Reduces Stainless Steel Corrosion. *J. Mater. Chem. A* **2014**, *2*, 18194−18198.
(27) Adams, B. D.; Radtke, C.; Black, R.; Trudeau, M. L.; Zaghib, K.; Nazar, L. F. Current Density Dependence of Peroxide Formation in the Li−O_2 Battery and its Effect on Charge. *Energy Environ. Sci.* **2013**, *6*, 1772−1778.
(28) Cheng, F.; Chen, J. Metal-air Batteries: From Oxygen Reduction Electrochemistry to Cathode Catalysts. *Chem. Soc. Rev.* **2012**, *41*, 2172−2192.
(29) Torres, W.; Mozhzhukhina, N.; Tesio, A. Y.; Calvo, E. J. A Rotating Ring Disk Electrode Study of the Oxygen Reduction Reaction in Lithium Containing Dimethyl Sulfoxide Electrolyte: Role of Superoxide. *J. Electrochem. Soc.* **2014**, *161*, A2204−A2209.
(30) Peng, Z.; Freunberger, S. A.; Hardwick, L. J.; Chen, Y.; Giordani, V.; Barde, F.; Novak, P.; Graham, D.; Tarascon, J. M.; Bruce, P. G. Oxygen Reactions in a Non-aqueous Li+ Electrolyte. *Angew. Chem., Int. Ed.* **2011**, *50*, 6351−6355.
(31) Laoire, C. O.; Mukerjee, S.; Abraham, K. M.; Plichta, E. J.; Hendrickson, M. A. Influence of Nonaqueous Solvents on the Electrochemistry of Oxygen in the Rechargeable Lithium−Air Battery. *J. Phys. Chem. C* **2010**, *114*, 9178−9186.
(32) Girishkumar, G.; McCloskey, B.; Luntz, A. C.; Swanson, S.; Wilcke, W. Lithium−Air Battery: Promise and Challenges. *J. Phys. Chem. Lett.* **2010**, *1*, 2193−2203.
(33) Read, J.; Mutolo, K.; Ervin, M.; Behl, W.; Wolfenstine, J.; Driedger, A.; Foster, D. Oxygen Transport Properties of Organic Electrolytes and Performance of Lithium/Oxygen Battery. *J. Electrochem. Soc.* **2003**, *150*, A1351−A1356.
(34) Lu, Y.-C.; Kwabi, D. G.; Yao, K. P. C.; Harding, J. R.; Zhou, J.; Zuin, L.; Shao-Horn, Y. The Discharge Rate Capability of Rechargeable Li−O_2 Batteries. *Energy Environ. Sci.* **2011**, *4*, 2999−3007.
(35) Quaranta, M.; Murkovic, M.; Klimant, I. A New Method to Measure Oxygen Solubility in Organic Solvents Through Optical Oxygen Sensing. *Analyst* **2013**, *138*, 6243−6245.
(36) Zhao-Karger, Z.; Zhao, X.; Fuhr, O.; Fichtner, M. Bisamide Based Non-Nucleophilic Electrolytes for Rechargeable Magnesium Batteries. *RSC Adv.* **2013**, *3*, 16330−16335.
(37) Mizrahi, O.; Amir, N.; Pollak, E.; Chusid, O.; Marks, V.; Gottlieb, H.; Larush, L.; Zinigrad, E.; Aurbach, D. Electrolyte Solutions with a Wide Electrochemical Window for Rechargeable Magnesium Batteries. *J. Electrochem. Soc.* **2008**, *155*, A103−A109.
(38) Guo, Y.; Zhang, F.; Yang, J.; Wang, F. Electrochemical Performance of Novel Electrolyte Solutions Based on Organoboron Magnesium Salts. *Electrochem. Commun.* **2012**, *18*, 24−27.
(39) Gizbar, H.; Vestfrid, Y.; Chusid, O.; Gofer, Y.; Gottlieb, H. E.; Marks, V.; Aurbach, D. Alkyl Group Transmetalation Reactions in Electrolytic Solutions Studied by Multinuclear NMR. *Organometallics* **2004**, *23*, 3826−3831.
(40) Park, M.; Zhang, X.; Chung, M.; Less, G. B.; Sastry, A. M. A Review of Conduction Phenomena in Li-ion Batteries. *J. Power Sources* **2010**, *195*, 7904−7929.
(41) Xu, K. Nonaqueous Liquid Electrolytes for Lithium-Based Rechargeable Batteries. *Chem. Rev.* **2004**, *104*, 4303−4417.
(42) Zhang, S. S.; Foster, D.; Read, J. Discharge Characteristic of a Non-aqueous Electrolyte Li/O_2 Battery. *J. Power Sources* **2010**, *195*, 1235−1240.
(43) Seyama, H.; Soma, M. X-ray Photoelectron Spectroscopic Study of Montmorillonite Containing Exchangeable Divalent Cations. *J. Chem. Soc., Faraday Trans. 1* **1984**, *80*, 237−248.
(44) Hallstedt, B. The Magnesium-Oxygen system. *CALPHAD: Comput. Coupling Phase Diagrams Thermochem.* **1993**, *17*, 281−286.
(45) Pour, N.; Gofer, Y.; Major, D. T.; Aurbach, D. Structural analysis of electrolyte solutions for rechargeable Mg batteries by stereoscopic means and DFT calculations. *J. Am. Chem. Soc.* **2011**, *133*, 6270−6278.
(46) de Waal, D.; Range, K.-J.; Königstein, M.; Kiefer, W. Raman Spectra of the Barium Oxide Peroxide and Strontium Oxide Peroxide Series. *J. Raman Spectrosc.* **1998**, *29*, 109−113.
(47) Born, M.; Huang, K. *Dynamical Theory of Crystal Lattices*; Oxford Press: Oxford, U. K., 1954; pp 367−373.

DOI: 10.1021/acs.chemmater.5b03608
Chem. Mater. 2015, 27, 7564−7568